Dalton Transactions

ROYAL SOCIETY OF CHEMISTRY

PAPER

View Article Online
View Journal | View Issue

Cite this: *Dalton Trans.*, 2025, **54**, 5311

Flexible bidentate aluminum Lewis acids for host–guest complex formation†

Tz-Ching Tsui,[a] Hao-Yuan Lan,[a] Han-Jung Li,[a] Ting-Shen Kuo[b] and Hsueh-Ju Liu *[a,c]

Received 25th November 2024,
Accepted 6th February 2025

DOI: 10.1039/d4dt03288h

rsc.li/dalton

This study investigates the design, synthesis, and reactivity of bidentate aluminum Lewis acids supported by amido and cyclopentadienyl donor sets within a flexible 1,4-disubstituted phenylene framework. The reactivity of these complexes with nitrogen-based ditopic donors was systematically explored, revealing their capacity to form host–guest assemblies. Reactions with equimolar pyrazine or quinoxaline yielded 1 : 1 colored adducts, highlighting the potential of these two systems as colorimetric sensors for ditopic nitrogen donors. The reaction with 4,4′-bipyridine, which features a longer N···N distance, resulted in a dimeric 2 : 2 adduct. In contrast, sterically demanding nitrogen donors such as 2,3,5,6-tetramethylpyrazine or phenazine showed no reactivity with these bidentate Lewis acids. The results reveal not only the robust Lewis acidic nature of the aluminum centers but also the pivotal role of ligand flexibility in facilitating diverse molecular interactions.

Introduction

Aluminum has long been recognized as a valuable Lewis acid in catalysis, owing to its low cost, high abundance, and versatile reactivity. Simple aluminum complexes including aluminum trihalides have been widely employed as catalysts or reagents in key organic reactions, including Friedel–Crafts alkylation and acylation, and the Meerwein–Ponndorf–Verley reduction.[1] These applications leverage the Lewis acidic nature of Al(III) ions and have laid a strong foundation for advancements in aluminum coordination chemistry. Building on these early studies, modern approaches focus on creating more sophisticated aluminum-based systems that enhance catalytic performance and broaden the scope of their applications.

One such advancement involves the strategic positioning of multiple Lewis acidic centers in close proximity, creating multidentate Lewis acidic sites within a single molecule. This concept parallels the use of multi-dentate ligands in coordination chemistry, where multiple donor groups provide enhanced binding capabilities to metal complexes. These multi-dentate Lewis acids show great promise in applications such as anion and molecular sensing and recognition[2] and catalysis for small molecule activation.[3] These studies underscore the potential of dual-site Lewis acids in cooperative binding and catalysis.

Our research builds on these concepts, focusing on multimetallic clusters that incorporate Lewis acidic centers. Recently, we reported a di-zinc framework supported by bisphenoxymethanone ligands, where synergistic interactions between the two zinc centers significantly enhanced reactivity in ε-caprolactone ring-opening polymerization compared to monomeric zinc complexes with similar coordination environments.[4] Additionally, we synthesized a unique anionic di-iron trihydride complex supported by a bis-cyclopentadienyl ligand, opening new avenues for heterobimetallic complex formation with coinage metals.[5] Inspired by these findings, we have turned our attention to aluminum-based bidentate Lewis acids, supported by amido and cyclopentadienyl donor sets within a di-substituted-1,4-C_6H_4 scaffold. Herein, we report the synthesis, structural characterization, and reactivity of these flexible di-aluminum systems, with a particular focus on their ability to form host–guest complexes.

Results and discussion

The synthesis of complexes **1-(Et$_2$O)$_2$** and **2-(Et$_2$O)$_2$** is outlined in Scheme 1, where **1** represents the **L1**-$(AlCl_2)_2$ moiety and **2** represents the **L2**-$(AlCl_2)_2$ moiety. Treatment of *in situ* prepared **Li$_2$L1** from **H$_2$L1** with 2.05 equiv. of $AlCl_3$ in diethyl ether at ambient temperature yielded **1-(Et$_2$O)$_2$** as a white solid in 86%

[a]*Department of Applied Chemistry, National Yang Ming Chiao Tung University, 1001 Daxue Rd, East District, Hsinchu City, Taiwan 300093.*
E-mail: hsuehjuliu@nycu.edu.tw
[b]*Department of Chemistry, National Taiwan Normal University, Taipei 11677, Taiwan*
[c]*Center for Emergent Functional Matter Science, National Yang Ming Chiao Tung University, 1001 Daxue Rd, East District, Hsinchu City, Taiwan 300093*

† Electronic supplementary information (ESI) available. CCDC 2390325, 2390330, 2390331, 2390335 and 2390401–2390405. For ESI and crystallographic data in CIF or other electronic format see DOI: https://doi.org/10.1039/d4dt03288h

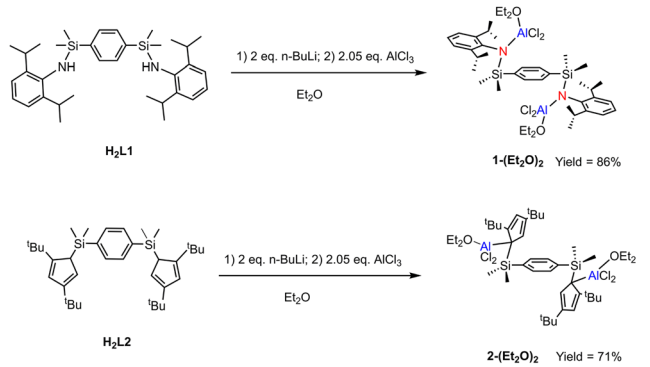

Scheme 1 Synthesis of **1-(Et$_2$O)$_2$** and **2-(Et$_2$O)$_2$**.

yield. Under similar conditions, using **H$_2$L2** afforded **2-(Et$_2$O)$_2$** in 71% yield.

The ^{1}H NMR spectra of both **1-(Et$_2$O)$_2$** and **2-(Et$_2$O)$_2$** confirmed the presence of coordinated Et$_2$O molecules (δ = 3.59 and 0.67 ppm for **1-(Et$_2$O)$_2$**; 3.53, 3.27, and 0.65 ppm for **2-(Et$_2$O)$_2$**), indicating the Lewis acidic nature of both complexes. Notably, the α-protons of the coordinated Et$_2$O in **2-(Et$_2$O)$_2$** are diastereotopic due to the asymmetric environment of aluminum centers in the **L2**-(AlCl$_2$)$_2$ moiety. Single-crystal X-ray diffraction analyses (see Fig. 1) provided the molecular structures of **1-(Et$_2$O)$_2$** and **2-(Et$_2$O)$_2$**, revealing that the two AlCl$_2$(OEt$_2$) moieties in each complex adopt a *trans*-conformation relative to the central *p*-phenylene spacer. Both aluminum centers in **1-(Et$_2$O)$_2$** and **2-(Et$_2$O)$_2$** exhibit tetrahedral geometry. The Al–N bond length of 1.798(7) Å in **1-(Et$_2$O)$_2$** and the Al–C (η^1-Cp coordination) bond length of 1.981(4) Å in **2-(Et$_2$O)$_2$** are consistent with those reported for four-coordinated aluminum amido[6] and Al(η^1-Cp)[7] complexes in the literature.

To evaluate the Lewis acidity of **1-(Et$_2$O)$_2$** and **2-(Et$_2$O)$_2$**, triethylphosphine oxide (TEPO) was employed as a probe molecule using the Gutmann–Beckett method.[8] Complexation reactions of **1-(Et$_2$O)$_2$** and **2-(Et$_2$O)$_2$** with 2 equiv. of TEPO resulted in similar changes in the ^{31}P chemical shift ($\Delta(\delta^{31}P)$ = +30.3 and +30.0 ppm for **1-(Et$_2$O)$_2$** and **2-(Et$_2$O)$_2$**, respectively, relative to the δ^{31}P of TEPO) in C$_6$D$_6$, indicating comparable Lewis acidity of **1** and **2** toward TEPO. The close Al–O bond lengths observed in the X-ray structures of **1-(Et$_2$O)$_2$** (1.884(7) Å) and **2-(Et$_2$O)$_2$** (1.872(3) Å) further confirm the similar Lewis acidity of the aluminum centers.

Given the Lewis acidic nature of **1-(Et$_2$O)$_2$** and **2-(Et$_2$O)$_2$**, various donor molecules were used to assess their coordination capabilities. Replacing the Et$_2$O ligand in **1-(Et$_2$O)$_2$** with the stronger donor 4-dimethylaminopyridine (DMAP) yielded colorless **1-(DMAP)$_2$** in 63% yield, demonstrating the potential of **1-(Et$_2$O)$_2$** as a useful precursor for host–guest chemistry. The crystal structure of **1-(DMAP)$_2$** is shown in Fig. 2a, featuring two AlCl$_2$(DMAP) moieties arranged in an anti-configuration relative to the central *p*-phenylene spacer, similar to the structure of **1-(Et$_2$O)$_2$**. Inspired by the work of Katz[9] and Mitzel,[10] which demonstrated that rigid bidentate boron Lewis acids serve as effective receptors for ditopic pyrimidine coordination, we envisioned that the bimetallic **1-(Et$_2$O)$_2$** and **2-(Et$_2$O)$_2$** might function as selective receptors for neutral Lewis bases. To explore this, we used pyrazine, which has a similar size to the central *p*-phenylene spacer in our bidentate Lewis acids, as a coordinating ligand in our study.

The reaction of **1-(Et$_2$O)$_2$** with 1 equiv. of pyrazine (pyz) in toluene rapidly generated an orange-red solution. The resulting product's ^{1}H NMR spectrum indicated clean formation of a new species as a 1 : 1 self-assembled adduct. Red crystals of **1-κ^2-pyz**, obtained by diffusing pentane into a saturated toluene solution, were characterized by single-crystal X-ray diffraction. The solid-state structure of **1-κ^2-pyz** reveals that two AlCl$_2$ fragments act as a bidentate Lewis acidic receptor for pyrazine binding, with the pyrazine molecule residing in the "binding pocket" in a **κ^2**-binding mode (see Fig. 2b). This supramolecule features Al–N$_{pyz}$ bond lengths of 2.000(2) and 2.022(2) Å, and an interplanar distance of 3.440 Å (centroid$_{pyz}$ to centroid$_{Ph}$) between the pyrazine and central *p*-phenylene ring. The short distance between the two aromatic planes suggests intramolecular π–π interactions. Similarly, **2-κ^2-pyz** was obtained from the reaction of **2-(Et$_2$O)$_2$** with 1 equiv. of pyrazine, affording a dark green solid in 95% yield. Structural analysis by X-ray diffraction (Fig. 2e) confirms the formation of a 1 : 1 adduct, with Al–N bond lengths of 2.024(2) and 2.029(2) Å, and a longer interplanar distance of 3.617 Å between the pyrazine and central *p*-phenylene spacer.

The intriguing color change observed when equimolar amounts of pyrazine react with the colorless precursors **1-(Et$_2$O)$_2$** and **2-(Et$_2$O)$_2$** to form **1-κ^2-pyz** and **2-κ^2-pyz**, respectively, highlights the potential utility of these complexes as sensors for detecting ditopic aromatic N-donors. This is particularly notable since Al^{3+} complexes are typically colorless, even when coordinated with pyrazine, as recently demonstrated by Müller-Buschbaum and coworkers, who reported the formation of predominantly colorless polymeric or dimeric complexes of AlCl$_3$ or InCl$_3$ with pyrazine as a bridging ligand.[11] These contrasting observations sparked our interest in understanding the origin of the color in our Al-pyrazine systems.

To investigate the host–guest interactions and electronic structures, titration experiments were performed using UV-vis spectroscopy. The colorless precursors **1-(Et$_2$O)$_2$** and **2-(Et$_2$O)$_2$**

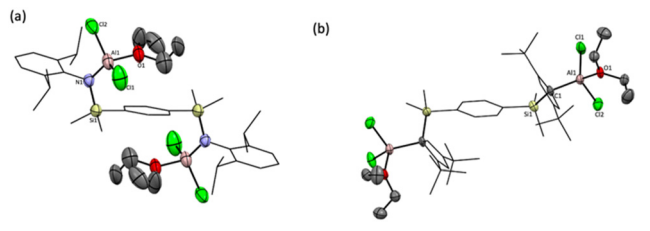

Fig. 1 Molecular structures of (a) **1-(Et$_2$O)$_2$** and (b) **2-(Et$_2$O)$_2$** (thermal ellipsoids drawn at the 50% probability level for Al, C, Si, N, and O; capped sticks representation for the ligand skeleton; H atoms have been omitted for clarity).

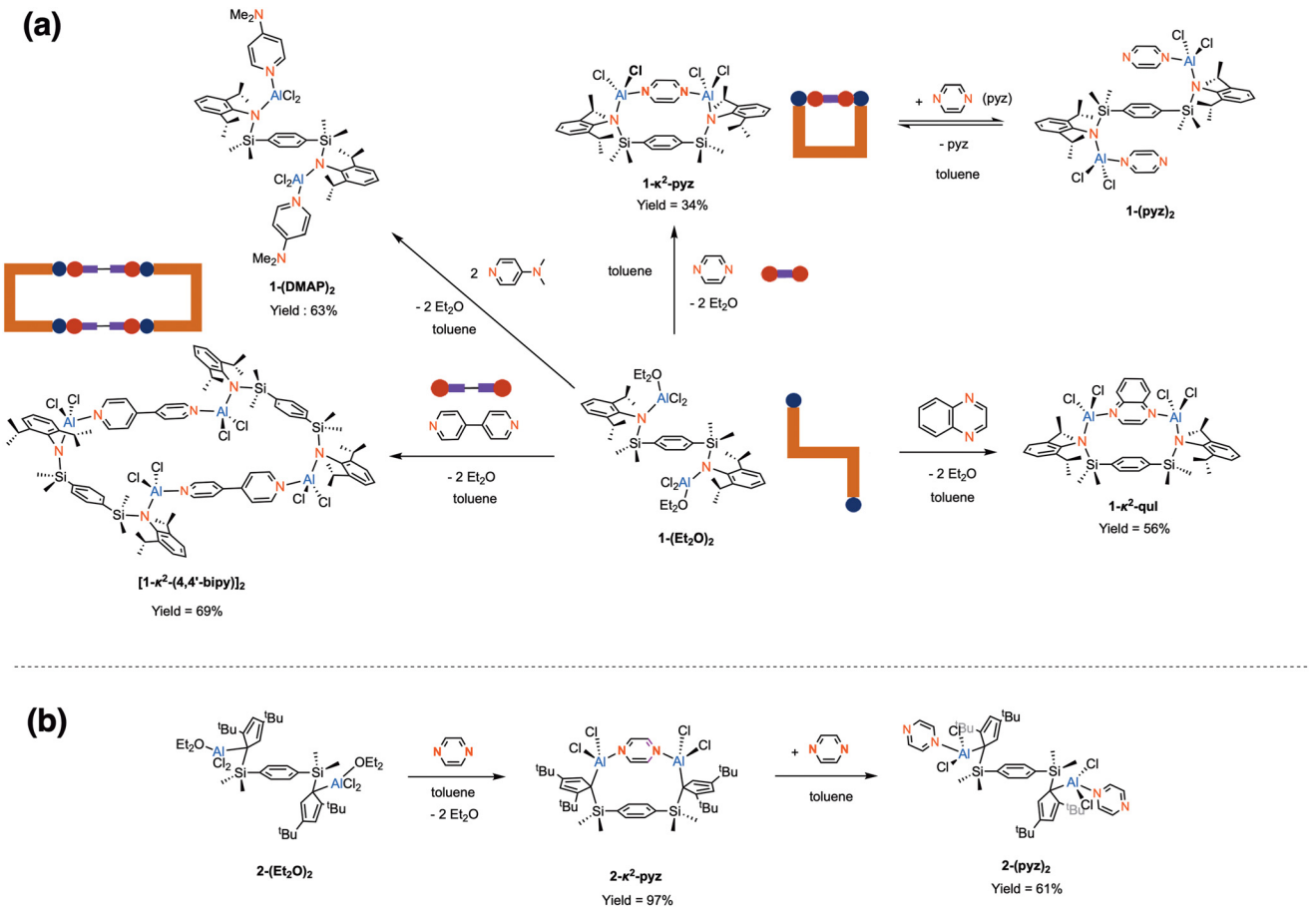

Scheme 2 Reactivity of (a) **1-(Et$_2$O)$_2$** and (b) **2-(Et$_2$O)$_2$**.

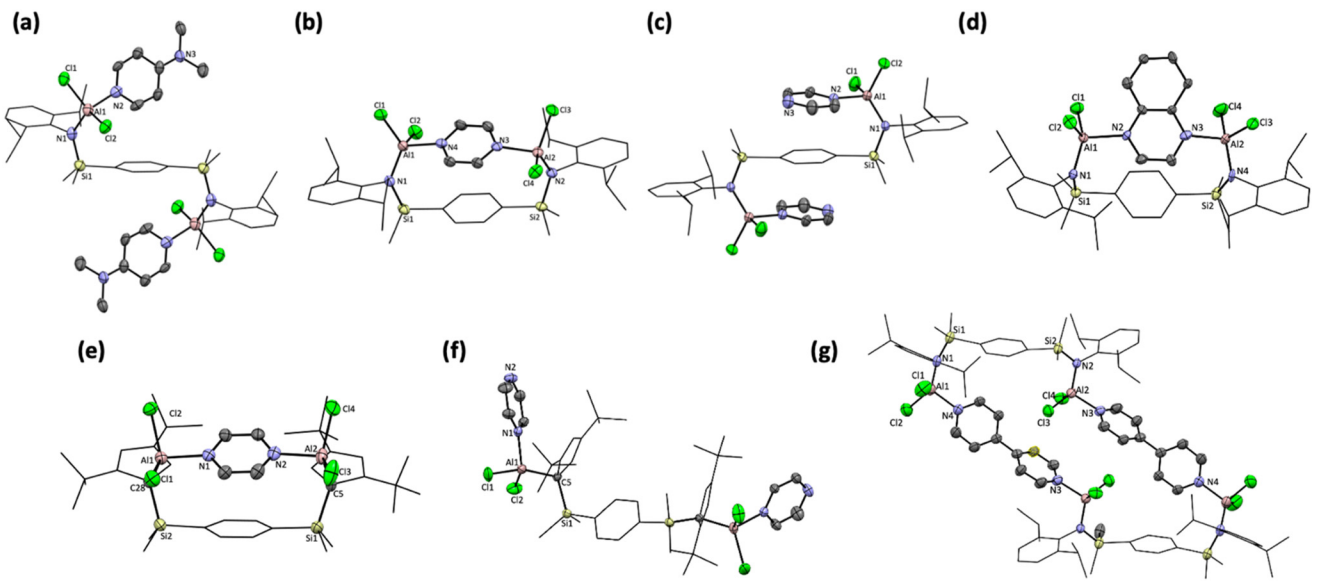

Fig. 2 ORTEP diagram showing the molecular structures of (a) **1-(DMAP)$_2$**, (b) **1-κ^2-pyz**, (c) **1-(pyz)$_2$**, (d) **1-κ^2-qul**, (e) **2-κ^2-pyz**, (f) **2-(pyz)$_2$**, and (g) **1$_2$-μ-(bipy)$_2$** (thermal ellipsoids drawn at the 50% probability level for Al, C, Si, N, and O; capped sticks representation for the ligand skeleton; H atoms have been omitted for clarity).

exhibit no noticeable absorption beyond 300 nm. For **1-$(Et_2O)_2$** (5×10^{-4} M), increasing the amount of pyrazine resulted in the appearance of a broad absorption band at 365 nm, which reached maximum intensity at a 1 : 1 stoichiometric ratio (Fig. 3a), consistent with the clean formation of **1-κ²-pyz** as confirmed by ^{1}H NMR spectroscopy. In the case of **2-$(Et_2O)_2$**, increasing the pyrazine concentration led to the appearance of a distinct absorption band at 570 nm, which also reached a maximum when 1 equiv. of pyrazine was added.

To gain further insights, the electronic structures of **1-κ²-pyz** and **2-κ²-pyz** were examined using DFT calculations. The results revealed that the HOMO and HOMO−1 in both systems primarily consist of the donor π-bonding orbitals of the 2,6-diisopropylphenyl groups (in **1-κ²-pyz**) or cyclopentadienyl groups (in **2-κ²-pyz**). Additionally, the *p*-phenylene π bonding orbitals appear as HOMO−6 and HOMO−6 in **1-κ²-pyz** and HOMO−4 and HOMO−5 in **2-κ²-pyz** (see Fig. S21 and S22†). The LUMO in both cases is dominated by the π* orbitals of pyrazine. The transitions from these occupied molecular orbitals to the LUMO likely account for the observed orange color in **1-κ²-pyz** and green color in **2-κ²-pyz** (see Fig. S21 and S22†).

Further reactivity studies revealed distinct behaviors for **1-κ²-pyz** and **2-κ²-pyz** when exposed to excess pyrazine. The reaction of **2-κ²-pyz** with additional equivalents of pyrazine in toluene resulted in a rapid color change from dark green to pale yellow, with ^{1}H NMR spectroscopy confirming the clean conversion to **2-(pyz)$_2$**. Single-crystal X-ray diffraction (Fig. 2f) revealed a *trans*-arrangement of two Cp*t*Bu$_2$AlCl$_2$(κ^1-pyz) fragments relative to the central *p*-phenylene spacer, with a slightly shorter Al–N(pyrazine) bond length of 1.979(4) Å compared to 2.024(2) and 2.029(2) Å in **2-κ²-pyz**. UV-vis titration experiments further supported this observation: upon addition of >1 equiv. of pyrazine, the 570 nm band decreased significantly and ultimately vanished when >2 equiv. of pyrazine was present (see Fig. 3b).

In contrast, the addition of 1 equiv. of pyrazine to **1-κ²-pyz** resulted in only ~62% conversion to **1-(pyz)$_2$**, as determined by ^{1}H NMR spectroscopy, indicating a dynamic equilibrium between **1-κ²-pyz** and pyrazine. Upon further addition of excess pyrazine (>3 equiv.), a yellow precipitate formed, which was identified as **1-(pyz)$_2$** *via* X-ray crystallography (Fig. 2c). This structure features a unique triple-decker stacking arrangement of pyrazine-*p*-phenylene-pyrazine with an interplanar distance of 3.614 Å (centroid$_{pyrazine}$ to centroid$_{phenylene}$). UV-vis titration experiments corroborated these findings, showing only ~30% reduction of the 365 nm band with a three-fold excess of pyrazine to **1-κ²-pyz**, consistent with the dynamic equilibrium observed in NMR. In contrast, an immediate reduction of the absorption band of **2-κ²-pyz** was observed upon the addition of a slight excess of pyrazine (Fig. 3a).

The observed differences between systems **1** and **2** can likely be attributed to variations in intramolecular π interactions between pyrazine and the central *p*-phenylene ring. Despite comparable Lewis acidity for **1** and **2**, as determined by the Gutmann–Beckett method, the *p*-phenylene-pyrazine π interaction appears to play a stabilizing role in **1-κ²-pyz**, result-

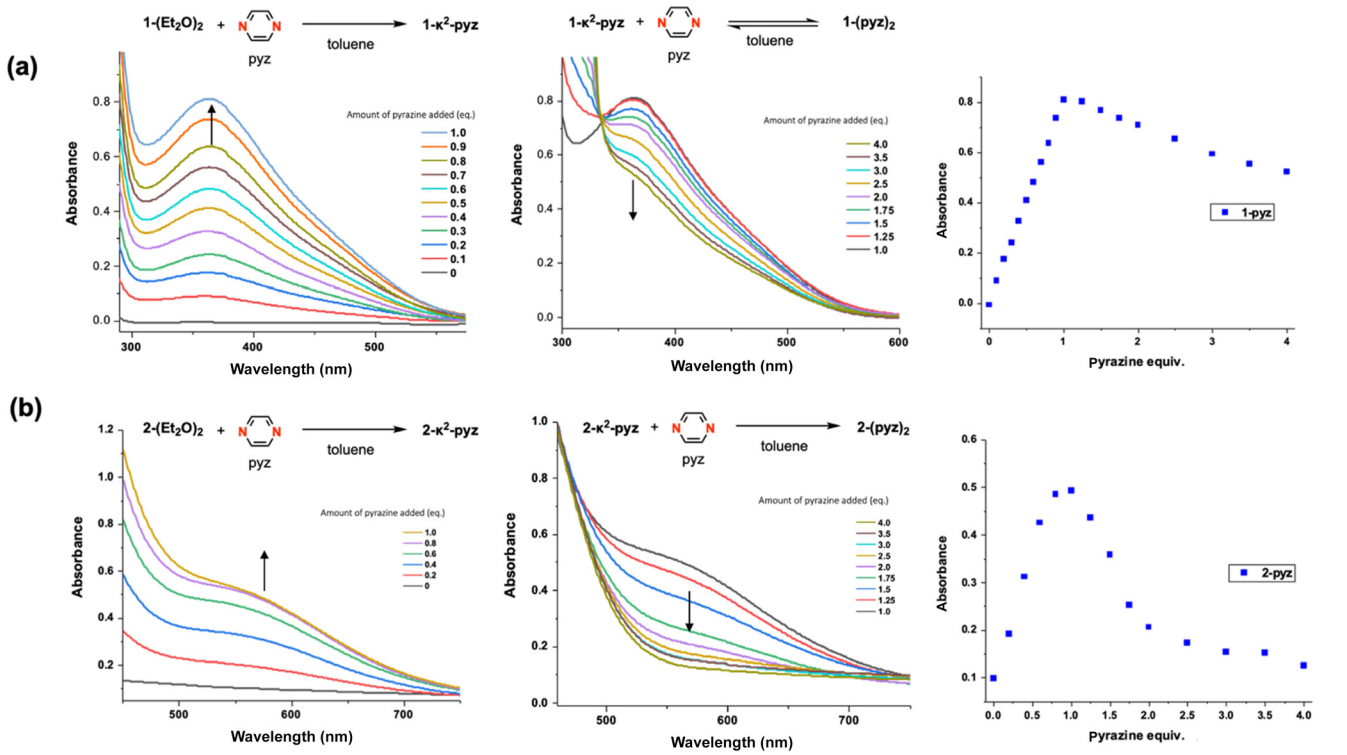

Fig. 3 UV-vis spectra and results showing the effects of varying amounts of pyrazine on (a) **1-$(Et_2O)_2$** and (b) **2-$(Et_2O)_2$**.

ing in its distinct reactivity profile. The distinct color changes observed when **1-(Et_2O)$_2$** and **2-(Et_2O)$_2$** react with pyrazine, along with their differing reactivities toward excess pyrazine, demonstrate the ability of these bidentate aluminum Lewis acids to interact selectively with ditopic nitrogen donors. Moreover, the resistance of **1-κ^2-pyz** to complete conversion to **1-(pyz)$_2$** in the presence of excess pyrazine suggests that **1-(Et_2O)$_2$** could serve as an ideal colorimetric sensor for pyrazine within a specific concentration range.

Examining the crystal structure of **1-κ^2-pyz**, we observe that while the pyrazine plane is not perfectly parallel to the central *p*-phenylene plane (with an interplanar angle of 14.7°), the pyrazine guest molecule resides well within the coordination pocket, attributed to its similar size to the central *p*-phenylene ring. Consequently, other ditopic nitrogen donors with comparable N···N distances to pyrazine should also serve as suitable guests for **1-(Et_2O)$_2$** and **2-(Et_2O)$_2$**. Due to the poor solubility of N-donor adducts with **2-(Et_2O)$_2$**, further studies with various N donors were conducted exclusively with **1-(Et_2O)$_2$**.

To explore the ability of **1-(Et_2O)$_2$** as a bidentate chelator for ditopic Lewis bases, several aromatic and aliphatic N donors were tested, including quinoxaline (qul), phenazine or 2,3,5,6-tetramethylpyrazine. Treatment of **1-(Et_2O)$_2$** with 1 equiv. of quinoxaline in toluene produced an orange-brown solid in 56% yield (Scheme 2a). The molecular structure of **1-κ^2-qul** was determined by X-ray crystallography, revealing Al–N_{qul} bond lengths of 2.031(7) and 2.033(8) Å, comparable to those in **1-κ^2-pyz** (Fig. 2d). Interestingly, the more sterically demanding quinoxaline, which contains an additional fused aromatic ring, resulted in a larger interplanar angle of 31.4° between the quinoxaline and central *p*-phenylene planes—significantly larger than the 14.7° angle observed in **1-κ^2-pyz**. To accommodate quinoxaline within the binding pocket of **1-(Et_2O)$_2$**, the two 2,6-diisopropylphenyl (dipp) groups were repositioned to one side, creating sufficient space for the inclined quinoxaline plane, as shown in Fig. S20.† This steric adjustment suggests the spatial constraints posed by bulkier guest molecules. Consequently, no reaction was observed between **1-(Et_2O)$_2$** and 1 equiv. of either phenazine or 2,3,5,6-tetramethylpyrazine, likely due to steric hindrance posed by these guest molecules.

In Mitzel's work,[10] the reaction of a rigid diborane system with 3,3′-bipyridine resulted in an insoluble product, likely a polymeric structure. Similarly, Wagner demonstrated that reactions of ferrocene-containing diborane with ditopic Lewis bases, such as pyrazine or 4,4′-bipyridine, resulted in the formation of coordination polymers.[12] In our previous research, a bidentate Lewis acidic di-zinc framework also reacted with 4,4′-bipyridine to produce a polymeric, ladder-type structure.[4] By contrast, the introduction of flexible $SiMe_2$ linkers in dinuclear organotin systems, as reported by Höpfl, Jurkschat, and coworkers, allows the formation of discrete 1 : 1 assemblies with substrates containing di-carboxylate or di-dithiocarbamate groups, suggesting the influence of structural flexibility on product formation.[2g]

In our current system, it is evident that 4,4′-bipyridine, with its extended N···N distance, does not fit within the defined binding pocket of **1-(Et_2O)$_2$**. This raises the intriguing possibility of an alternative binding mode, potentially involving the formation of intermolecular superstructures. To explore this, the reaction between **1-(Et_2O)$_2$** and 4,4′-bipyridine was carried out. Upon addition of 4,4′-bipyridine to a toluene solution of **1-(Et_2O)$_2$**, light yellow precipitates formed immediately. By carefully layering a toluene solution of 4,4′-bipyridine over a solution of **1-(Et_2O)$_2$**, we allowed for slow diffusion between the layers, which effectively yielded crystals suitable for single-crystal X-ray diffraction analysis (see Fig. 2g). The resulting molecular structure revealed the formation of a 2 : 2 adduct, **1$_2$-μ-(bipy)$_2$**, where two equiv. of **1-(Et_2O)$_2$** and 4,4′-bipyridine assemble into a dimer. This unexpected dimerization highlights the flexibility of the $SiMe_2$ linkages in the ligand system, enabling the formation of an intermolecular complex. The Al–N distances in **1$_2$-μ-(bipy)$_2$** are approximately 1.96 Å, which is notably shorter than the Al–N distance observed in **1-κ^2-pyz** (2.02 Å), further underscoring the adaptability of the framework in accommodating various guest molecules.

Conclusions

The design of a ditopic ligand within the 1,4-$(SiMe_2)_2C_6H_4$ disubstituted framework creates the flexibility and adaptability of the bidentate aluminum Lewis acid framework, exemplified by **1-(Et_2O)$_2$** and **2-(Et_2O)$_2$**. These two systems demonstrate the capacity to accommodate a variety of nitrogen-based ditopic donors, each with distinct structural demands. These findings underscore the potential of **1-(Et_2O)$_2$** and similar frameworks in promoting tailored host–guest interactions. By accommodating guest molecules with varying steric and spatial requirements, this system expands the possibilities for designing flexible and cooperative Lewis acid frameworks that could be leveraged in supramolecular chemistry, sensing, and small-molecule capture applications. This study opens pathways for further exploration of ditopic Lewis acids with adjustable binding sites, potentially enhancing reactivity and selectivity in targeted applications.

Experimental

General considerations

All manipulations with oxygen and moisture-sensitive materials were performed in a nitrogen-filled glovebox. Solvents were dried and deaerated using a solvent system (AsiaWong Enterprise Co., Ltd) prior to use. Benzene-d_6 was dried over sodium and benzophenone, degassed *via* three freeze–pump–thaw cycles, and stored under nitrogen over 3 Å molecular sieves. $CDCl_3$ was dried over 3 Å molecular sieves, degassed *via* three freeze–pump–thaw cycles, and stored under nitrogen. The NMR spectra were recorded using Bruker 300, Varian 400 or Varian 600 MHz spectrometers. The NMR spectra were referenced to residual protonated solvent for ^{1}H NMR (7.16 ppm for the compound in benzene-d_6; 7.26 ppm

for the compound in $CDCl_3$) and to deuterated solvent for ^{13}C NMR (128.06 for the compound in benzene-d_6; 77.16 ppm for the compound in $CDCl_3$). All spectra were recorded at 25 °C. Complex multiplets are denoted as "m" and broad resonances as "br". Elemental analyses were performed using an Elementar vario EL CUBE (CHN-OS Rapid, Germany). Mass spectrometry was performed using a JMS-T200GC AccuTOF GCx (source mode: FD (field desorption)). Di-*tert*-butylcyclopentadiene ($Cp^{tBu2}H$), its deprotonated form $Cp^{tBu2}Li$[13] and *p*-$Ph(SiMe_2Cl)_2$[14] were synthesized according to the reported procedures.

Synthesis of LiNHDipp (Dipp = 2,6-diisopropylphenyl). Commercially available 2,6-diisopropylaniline ($DippNH_2$) was dried over 3 Å molecular sieves, degassed using three freeze–pump–thaw cycles, and stored under nitrogen. A solution of *n*-BuLi (1.6 M in hexane, 43 mL, 68.7 mmol) was slowly added to a pre-cooled (−35 °C) 200 mL pentane solution of $DippNH_2$ (12.8 g, 72.3 mmol). The mixture was then allowed to warm to room temperature and stirred for 18 h, resulting in the formation of a white precipitate. The precipitate was filtered and washed with 20 mL of pentane, yielding 12.5 g of white powder (LiNHDipp) after drying. Yield: ∼100%.

Synthesis of H_2L1. An Et_2O solution (100 mL) of LiNHDipp (3.48 g, 19.0 mmol) was slowly added to a solution of p-Ph$(SiMe_2Cl)_2$ (2.50 g, 9.49 mmol) in Et_2O (100 mL) at −35 °C. After stirring at ambient temperature for 18 h, the volatile components were removed under vacuum, and the product was extracted with pentane (70 mL). The pentane solution was filtered, and the solvent was removed under reduced pressure, yielding **H_2L1** as a white powder (5.10 g, 99%). **^{1}H NMR** (400 MHz, benzene-d_6, 298 K): δ 7.63 (s, 4H, *Ph*H), 7.06–7.14 (m, 6H, *DippH*), 3.43 (m, 4H, i*Pr*), 2.49 (s, 2H, *NH*), 1.16 (d, J = 6.78 Hz, 24H, i*Pr*), 0.34 (s, 12H, *SiMe$_2$*) ppm. **^{13}C{^{1}H} NMR** (100 MHz, benzene-d_6, 298 K): δ 144.1, 141.1, 139.6, 132.9, 124.2, 123.5, 28.7, 23.8, −0.7 ppm. Elemental analysis calcd (%) for $C_{34}H_{52}N_2Si_2$: C 74.93, N 5.14, H 9.62. Found: C 74.85, N 5.08, H 9.43.

Synthesis of H_2L2. A THF solution (20 mL) of $Cp^{tBu2}Li$ (3.00 g, 16.3 mmol) was slowly added to a solution of p-Ph$(SiMe_2Cl)_2$ (2.10 g, 8.00 mmol) in THF (30 mL) at −35 °C. After stirring at room temperature for 18 h, the volatile components were removed under vacuum, and the product was extracted with pentane (70 mL). The pentane solution was concentrated to approximately 15 mL under reduced pressure and then cooled in a −35 °C freezer to yield **H_2L2** as a white powder (3.28 g, 75%) composed of a mixture of π-bond positional isomers. **^{1}H NMR** (400 MHz, $CDCl_3$, 298 K): δ = 7.51 (s, 4H, *PhH*), 6.37 (s, 2H, *CpH*), 5.67 (br, 2H, *CpH*), 3.51 (br, 2H, *CpH*), 1.11 (s, 36H, *tBu*), 0.23 (s, 12H, *SiMe$_2$*) ppm. **^{13}C{^{1}H} NMR** (100 MHz, $CDCl_3$, 298 K): δ = δ 141.2, 133.0, 125.4, 77.2, 33.0, 31.1, −2.7 ppm. Elemental analysis calcd (%) for $C_{36}H_{58}Si_2$: C 79.04, H 10.69. Found: C 79.06, H 10.83.

Synthesis of L1[$AlCl_2$(Et_2O)]$_2$ (1-(Et_2O)$_2$). A solution of *n*-BuLi (1.6 M in hexane, 6.7 mL, 10.7 mmol) was slowly added to a pre-cooled (−35 °C) 80 mL pentane solution of **H_2L1** (3.00 g, 5.5 mmol). The mixture was then allowed to warm to room temperature and stirred for 18 h, resulting in the formation of a white precipitate. The precipitate was filtered and washed with 20 mL of pentane, yielding 2.89 g of white powder (**Li_2L1**) after drying. Yield: 97%.

A suspension of $AlCl_3$ (0.144 g, 1.11 mmol) in 10 mL of Et_2O was added to the **Li_2L1** (0.300 g, 0.54 mmol) solution in Et_2O (10 mL) at −35 °C. The mixture was then allowed to warm to room temperature and stirred for 18 h. Afterward, the volatile components were removed under vacuum, and the product was extracted with 20 mL of toluene. The mixture was filtered, and the volatiles were removed *in vacuo* to afford white powder **L1[$AlCl_2$(Et_2O)]$_2$ (1-(Et_2O)$_2$)**. Yield: 0.422 g, 88%. **^{1}H NMR** (400 MHz, benzene-d_6, 298 K): δ 7.86 (s, 4H, *Ph*), 7.15–7.11 (m, 6H, *Dipp*), 3.93 (m, 4H, *CH*Me$_2$), 3.59 (q, J = 7.04 Hz, 8H, O(C*H*$_2$CH$_3$)$_2$), 1.39–1.30 (m, 24H, CH*Me*$_2$), 0.67 (t, J = 6.98 Hz, 12H, O(CH$_2$C*H*$_3$)$_2$), 0.34 (s, 12H, *SiMe$_2$*) ppm. **^{13}C{^{1}H} NMR** (100 MHz, benzene-d_6, 298 K): δ 146.9, 143.1, 142.1, 134.3, 124.7, 124.4, 69.7, 28.1, 25.9, 25.2, 12.9, 1.0 ppm. Anal. calcd for $C_{42}H_{70}Al_2Cl_4N_2O_2Si_2$: C 56.87, H 7.96, N 3.16. Found: C 57.33, H 8.21, N 3.40.

Synthesis of L2[$AlCl_2$(Et_2O)]$_2$ (2-(Et_2O)$_2$). A solution of **H_2L2** (2.60 g, 4.75 mmol) in 70 mL of pentane was treated with *n*-BuLi (1.6 M in hexane, 5.90 mL, 9.50 mmol) at room temperature, and the mixture was stirred for 18 h. Afterward, the volatile components were removed under vacuum as much as possible, and the resulting yellow, viscous oil was treated with 50 mL of Et_2O, yielding **Li_2L2** as a white solid (2.57 g, 77%).

A suspension of $AlCl_3$ (0.387 g, 2.90 mmol) in 10 mL of Et_2O was added to the **Li_2L2** (1.00 g, 1.41 mmol) solution in Et_2O (10 mL) at −35 °C. The mixture was then allowed to warm to room temperature and stirred for 18 hours. After this period, the mixture was filtered, and the filtrate was concentrated to about 1–2 mL under vacuum. The concentrated ether solution was carefully layered with 10 mL of pentane and cooled to −35 °C, yielding a white solid **L2[$AlCl_2$(Et_2O)]$_2$ (2-(Et_2O)$_2$)**, after drying. Yield: 0.893 g, 71%. **^{1}H NMR** (400 MHz, benzene-d_6, 298 K): δ = 7.55–7.52 (br, 4H, *Ph*), 6.80 (s, 2H, *CpH*), 6.36 (s, 2H, *CpH*), 3.53 (br, 2H, O(C*H*$_2$CH$_3$)$_2$), 3.27 (br, 2H, O(C*H*$_2$CH$_3$)$_2$), 1.47 (s, 18H, *tBu*), 1.29 (s, 18H, *tBu*), 0.88 (s, 6H, *SiMe$_2$*), 0.65 (br, 12H, O(CH$_2$C*H*$_3$)$_2$), 0.50 (s, 6H, *SiMe$_2$*) ppm. **^{13}C{^{1}H} NMR** (100 MHz, $CDCl_3$, 298 K): δ = 161.6, 153.1, 141.3, 141.2, 133.8, 128.1, 126.6, 123.5, 123.4, 68.7, 68.6, 34.7, 33.9, 32.6, 31.3, 12.8, 12.7, 3.2, 3.1, −1.3 ppm. Elemental analysis calcd (%) for $C_{44}H_{76}Al_2Cl_4O_2Si_2$: C 59.45, H 8.62. Found: C 59.51, H 8.16.

Synthesis of L1[$AlCl_2$(DMAP)]$_2$ (1-(DMAP)$_2$). Slow layering of a 5 mL toluene solution of 4-dimethylaminopyridine (27.5 mg, 0.226 mmol) onto a 5 mL toluene solution of **1-(Et_2O)$_2$** (100.0 mg, 0.113 mmol) resulted in the formation of colorless crystals of **1-(DMAP)$_2$** after 1 day. The crystals were collected, washed twice with 3 mL portions of toluene, and dried. Yield: 69.8 mg (63%). **^{1}H NMR** (400 MHz, $CDCl_3$, 298 K): δ 7.73 (d, 4H, ^3J = 6.90 Hz, *DMAP*) 7.52 (s, 4H, *Ph*), 7.09–7.04 (m, 6H, *Dipp*), 6.29 (d, 4H, $^3J_{H,H}$ = 6.90 Hz, *DMAP*), 3.74 (m, 4H, *CH*Me$_2$), 3.06 (s, 12H, N*Me$_2$*), 1.25 (d, 12H, ^3J = 6.84 Hz, CH*Me$_2$*), δ 1.12 (d, 12H, ^3J = 6.84 Hz, CH*Me$_2$*), 0.27 (s, 12H, *SiMe$_2$*) ppm. Satisfactory ^{13}C NMR data were not obtained due

to the poor solubility of **1-(DMAP)$_2$** in $CDCl_3$. Anal. calcd for $C_{48}H_{70}Al_2Cl_4N_6Si_2$: C 58.65, N 8.55, H 7.18. Found: C 59.18, N 8.33, H 7.34.

Synthesis of L1[AlCl$_2$]$_2$(κ^2-pyrazine) (1-κ^2-pyz). Pyrazine (9 mg, 0.113 mmol) was slowly added to a 5 mL toluene solution of **1-(Et$_2$O)$_2$** (100 mg, 0.113 mmol), causing the solution to quickly change from colorless to deep red. After stirring at room temperature for 3 h, the volatile components were removed under vacuum, yielding an orange-red crude product. The crude product (47.8 mg) was dissolved in 1–2 mL of toluene and filtered to remove any insoluble material. The filtrate was then carefully layered with 10 mL of pentane for crystallization, yielding X-ray quality orange-red crystals. Yield: 31.4 mg, 34%. **^{1}H NMR** (400 MHz, benzene-d_6, 298 K): δ 8.22 (s, 4H, *pyz*), 7.21–7.17 (m, 6H, *Dipp*), 7.14–7.05 (br, 4H, *Ph*), 4.95 (br, 4H, *CH*Me$_2$), 1.50 (d, 12H, J = 6.40 Hz, *CHMe$_2$*), 1.42 (d, 12H, J = 6.77 Hz, *CHMe$_2$*), 0.42 (br, 12H, *SiMe$_2$*) ppm. **^{13}C{^{1}H} NMR** (100 MHz, benzene-d_6, 298 K): δ 146.5, 144.5, 142.4, 142.3, 133.6, 125.2, 124.6, 28.4, 25.8, 24.8, −0.43 ppm. Elemental analysis calcd (%) for $C_{38}H_{54}Al_2Cl_4N_4Si_2$: C 55.74, N 6.84, H 6.65. Found: C 55.51, N 6.60, H 6.69. UV-vis: 365 (ε = 1600) in toluene.

Synthesis of L2[AlCl$_2$]$_2$(κ^2-pyrazine) (2-κ^2-pyz). Pyrazine (9 mg, 0.113 mmol) was slowly added to a 5 mL toluene solution of **2-(Et$_2$O)$_2$** (100 mg, 0.113 mmol), causing the solution to quickly change from colorless to deep green. After stirring at room temperature for 3 h, the volatile components were removed under vacuum, yielding a green crude product. The crude product was dissolved in 1–2 mL of toluene and filtered to remove any insoluble material. The filtrate was then carefully layered with 10 mL of pentane for crystallization, yielding X-ray quality dark green crystals. Yield: 90.0 mg (97%). **^{1}H NMR** (400 MHz, benzene-d_6, 298 K): δ 8.60 (br, 2H, *pyz*), 8.08 (br, 2H, *pyz*), 7.21–7.17 (m, 6H, *Dipp*), 7.10 (s, 4H, *Ph*), 6.94 (s, 2H, CpH), 5.17 (s, 2H, CpH), δ 5.17 (s, 2H, *He*), 1.66 (s, 18H, *tBu*), 1.34 (s, 18H, *tBu*), δ 0.98 (s, 6H, *SiMe$_2$*), δ 0.24 (s, 6H, *SiMe$_2$*). Satisfactory ^{13}C NMR data were not obtained due to the poor solubility of **2-κ^2-pyz** in C_6D_6. Repeated attempts at combustion elemental analysis did not produce satisfactory results. UV-vis: 570 (ε = 250) in toluene.

Synthesis of L1[AlCl$_2$(pyrazine)$_2$] (1-(pyz)$_2$). An excess of pyrazine (54.0 mg, 0.675 mmol) was added to a 5 mL toluene solution of **1-(Et$_2$O)$_2$** (60.0 mg, 0.068 mmol). The mixture was stirred at room temperature for 16 hours, after which the solution was filtered and concentrated under vacuum to a volume of approximately 1–2 mL. Pentane (10 mL) was then layered onto the concentrated solution, resulting in the formation of yellow crystals. The crystals were collected and dried, yielding 10.1 mg (16%).

Synthesis of L2[AlCl$_2$(pyrazine)$_2$] (2-(pyz)$_2$). Pyrazine (18.0 mg, 0.225 mmol) was added to a 5 mL toluene solution of **2-(Et$_2$O)$_2$** (100 mg, 0.113 mmol). The mixture was stirred at room temperature for 18 hours, after which the solution was filtered and concentrated under vacuum to a volume of approximately 1–2 mL. Pentane (10 mL) was then layered onto the concentrated solution, resulting in the formation of yellow crystals. The crystals were collected and dried, yielding 62.0 mg (61%). **^{1}H NMR** (400 MHz, C_6D_6): δ 7.94 (br, 4H, *pyz*), 7.73 (br, 4H, *pyz*), 7.25 (s, 4H, *Ph*), 6.57 (d, 2H, ^4J = 1.95 Hz, CpH), 6.22 (d, 2H, ^4J = 1.95 Hz, CpH), 1.39 (s, 18H, *tBu*), 0.99 (s, 18H, *tBu*), δ 0.88 (s, 6H, *SiMe$_2$*), δ 0.73 (s, 6H, *SiMe$_2$*) ppm. **^{13}C{^{1}H} NMR** (100.6 MHz, C_6D_6): δ 161.6, 153.7, 147.3, 141.9, 139.9, 133.4, 126.4, 122.2, 34.7, 33.9, 32.2, 30.9, 3.8, −0.6 ppm. Elemental analysis calcd (%) for $C_{44}H_{64}Al_2Cl_4N_4Si_2$: C 58.66, N 6.22, H 7.16. Found: C 58.61, N 5.86, H 7.03.

Synthesis of L1[AlCl$_2$]$_2$(κ^2-quinoxaline) (1-κ^2-qul). Quinoxaline (7.3 mg, 0.056 mmol) was slowly added to the 5 mL toluene solution of **1-(Et$_2$O)$_2$** (50 mg, 0.056 mmol), causing the solution to quickly change from colorless to yellow-orange. After stirring at room temperature for 18 h, the volatile components were removed under vacuum, yielding an orange crude product. The crude product was dissolved in 1–2 mL of toluene and filtered to remove any insoluble material. The filtrate was then carefully layered with 10 mL of pentane for crystallization, yielding X-ray quality orange-red crystals. Yield: 27.5 mg, 56%. **^{1}H NMR** (400 MHz, benzene-d_6, 343 K): δ 9.00 (m, 2H, *qul*), 8.82 (s, 2H, *qul*), 7.43 (s, 4H, *Ph*), 7.25–7.17 (m, 6H, *Dipp*), 7.06–7.00 (m, 2H, *qul*), 3.98 (br, 4H, ^3J = 6.75 Hz, *CH*Me$_2$), 1.47 (d, 12H, ^3J = 6.73 Hz, *CHMe$_2$*), δ 1.40 (br, 12H, *CHMe$_2$*), δ 0.51 (s, 12H, *SiMe$_2$*) ppm. **^{13}C{^{1}H} NMR** (100 MHz, benzene-d_6, 298 K): δ 143.8, 143.4, 143.3, 138.8, 134.3, 134.0, 127.5, 125.2, 29.1, 25.7, 0.6 ppm. Elemental analysis calcd (%) for $C_{42}H_{56}Al_2Cl_4N_4Si_2$: C 58.06, N 6.45, H 6.50. Found: C 58.16, N 6.38, H 6.37.

Synthesis of {L1[AlCl$_2$]$_2$}$_2$(μ-4,4′-bipyridine)$_2$ (1$_2$-μ-(bipy)$_2$). Slow layering of a 5 mL toluene solution of 4,4′-bipyridine (17.6 mg, 0.113 mmol) onto a 5 mL toluene solution of **1-(Et$_2$O)$_2$** (100.0 mg, 0.113 mmol) resulted in the formation of pale yellow crystals of **1$_2$-μ-(bipy)$_2$** after 1 day. The crystals were collected, washed twice with 3 mL portions of toluene, and dried. Yield: 69.6 mg (69%). **^{1}H NMR** (400 MHz, $CDCl_3$, 298 K): δ 8.47 (br, 8H, *bipy*), 7.81 (s, 8H, *Ph*), 7.80–7.78 (br, 8H, *bipy*), 7.12–7.00 (m, 12H, *Dipp*), 3.69 (m, 8H, *CH*Me$_2$), 1.22 (m, 24H, *CHMe$_2$*), 0.89 (m, 24H, *CHMe$_2$*), 0.32 (s, 24H, *SiMe$_2$*) ppm. Satisfactory ^{13}C NMR data were not obtained due to the poor solubility of **1$_2$-μ-(bipy)$_2$** in $CDCl_3$. Anal. calcd for $C_{95}H_{124}Al_4Cl_8N_8Si_4$ (**1$_2$-μ-(bipy)$_2$·toluene**): C 60.63, N 5.95, H 6.64. Found: C 60.83, N 5.67, H 6.70.

UV titration experiments

A 0.5 mL aliquot of a stock solution of **1-(Et$_2$O)$_2$** or **2-(Et$_2$O)$_2$** (5.0×10^{-3} M in toluene) was measured and mixed with varying amounts of pyrazine (2.5×10^{-3} M, 0–4 equivalents relative to **1-(Et$_2$O)$_2$** or **2-(Et$_2$O)$_2$**) in a 5 mL volumetric flask. Toluene was then added to bring the total volume to 5 mL. The UV-vis spectra were recorded using a quartz cuvette (5.0 mL capacity and 1 cm path length).

Data availability

The data supporting this article have been included as part of the ESI.†

Conflicts of interest

There are no conflicts to declare.

Acknowledgements

We thank Dr. Li-Ching Shen (Center for Advanced Instrumentation at NYCU) for assistance with NMR experiments. This work is also supported by the Center for Emergent Functional Matter Science of National Yang Ming Chiao Tung University through The Featured Areas Research Center Program within the framework of the Higher Education Sprout Project by the Ministry of Education (MOE) in Taiwan.

References

1 H. Meerwein, G. Hinz, H. Majert and H. Sönke, *J. Prakt. Chem.*, 1936, **147**, 226–250.
2 (*a*) S. Solé and F. P. Gabbaï, *Chem. Commun.*, 2004, 1284–1285; (*b*) V. Amendola, M. Bonizzoni, D. Esteban-Gómez, L. Fabbrizzi, M. Licchelli, F. Sancenón and A. Taglietti, *Coord. Chem. Rev.*, 2006, **250**, 1451–1470; (*c*) C. R. Wade, A. E. J. Broomsgrove, S. Aldridge and F. P. Gabbaï, *Chem. Rev.*, 2010, **110**, 3958–3984; (*d*) L. Gai, J. Mack, H. Lu, T. Nyokong, Z. Li, N. Kobayashi and Z. Shen, *Coord. Chem. Rev.*, 2015, **285**, 24–51; (*e*) E. Galbraith and T. D. James, *Chem. Soc. Rev.*, 2010, **39**, 3831–3842; (*f*) D. Dakternieks, K. Jurkschat, H. Zhu and E. R. T. Tiekink, *Organometallics*, 1995, **14**, 2512–2521; (*g*) I. Rojas-León, H. Alnasr, K. Jurkschat, M. G. Vasquez-Ríos, G. Gómez-Jaimes, H. Höpfl, I. F. Hernández-Ahuactzí and R. Santillan, *Organometallics*, 2019, **38**, 2443–2460; (*h*) V. Sharma, M. Simard and J. D. Wuest, *J. Am. Chem. Soc.*, 1992, **114**, 7931–7933; (*i*) P. L. Lückert, J. Gilmer, A. Virovets, H.-W. Lerner and M. Wagner, *Chem. Sci.*, 2025, **16**, 147–155.
3 (*a*) S. N. Kessler, M. Neuburger and H. A. Wegner, *Eur. J. Org. Chem.*, 2011, 3238–3245; (*b*) L. Hong, S. Ahles, A. H. Heindl, G. Tiétcha, A. Petrov, Z. Lu, C. Logemann and H. A. Wegner, *Beilstein J. Org. Chem.*, 2018, **14**, 618–625; (*c*) A. Lorbach, M. Bolte, H.-W. Lerner and M. Wagner, *Chem. Commun.*, 2010, **46**, 3592–3594; (*d*) T. Ooi, M. Takahashi and K. Maruoka, *J. Am. Chem. Soc.*, 1996, **118**, 11307–11308.
4 D.-H. Wu, X.-J. Lin, W. Benchaphanthawee, Y.-H. Lee, Z.-C. Lin, H.-J. Li, P.-L. Chen, T.-S. Kuo, C.-L. Wang, Y.-K. Wu, C.-H. Peng and H.-J. Liu, *ChemPlusChem*, 2024, e202400382.
5 C.-C. Tseng, Y.-W. Ding, Z.-Y. Chen, H.-Y. Lan, H.-J. Li, Y.-S. Cheng, T.-S. Kuo, P.-L. Chen, W.-C. Wu, F.-K. Shi, T. Yang and H.-J. Liu, *Inorg. Chem.*, 2024, **63**, 11361–11368.
6 (*a*) M. Schiefer, H. Hatop, H. W. Roesky, H.-G. Schmidt and M. Noltemeyer, *Organometallics*, 2002, **21**, 1300–1303; (*b*) M. Schiefer, N. D. Reddy, H.-J. Ahn, A. Stasch, H. W. Roesky, A. C. Schlicker, H.-G. Schmidt, M. Noltemeyer and D. Vidovic, *Inorg. Chem.*, 2003, **42**, 4970–4976.
7 P. E. Romero, W. E. Piers, S. A. Decker, D. Chau, T. K. Woo and M. Parvez, *Organometallics*, 2003, **22**, 1266–1274.
8 (*a*) U. Mayer, V. Gutmann and W. Gerger, *Chem. Mon.*, 1975, **106**, 1235–1257; (*b*) V. Gutmann, *Coord. Chem. Rev.*, 1976, **18**, 225–255; (*c*) M. A. Beckett, G. C. Strickland, J. R. Holland and K. Sukumar Varma, *Polymer*, 1996, **37**, 4629–4631.
9 H. E. Katz, *J. Org. Chem.*, 1989, **54**, 2179–2183.
10 P. Niermeier, S. Blomeyer, Y. K. J. Bejaoui, J. L. Beckmann, B. Neumann, H.-G. Stammler and N. W. Mitzel, *Angew. Chem., Int. Ed.*, 2019, **58**, 1965–1969.
11 T. C. Schäfer, J. Becker, D. Heuler, M. T. Seuffert, A. E. Sedykh and K. Müller-Buschbaum, *Aust. J. Chem.*, 2022, **75**, 676–683.
12 (*a*) M. Fontani, F. Peters, W. Scherer, W. Wachter, M. Wagner and P. Zanello, *Eur. J. Inorg. Chem.*, 1998, **1998**, 1453–1465; (*b*) M. Grosche, E. Herdtweck, F. Peters and M. Wagner, *Organometallics*, 1999, **18**, 4669–4672.
13 C. E. Zachmanoglou, J. G. Melnick, B. M. Bridgewater, D. G. Churchill and G. Parkin, *Organometallics*, 2005, **24**, 603–611.
14 K. Reuter, R. G. M. Maas, A. Reuter, F. Kilgenstein, Y. Asfaha and C. von Hänisch, *Dalton Trans.*, 2017, **46**, 4530–4541.